Investigation of dynamic change in microplastics vertical distribution patterns: The seasonal effect on vertical distribution

Cristele Chevalier, Marine Vandenberghe, Marc Pagano, Ian Pellet, Christel Pinazo, Javier Tesán Onrubia, Loïc Guilloux, François Carlotti

▶ **To cite this version:**

Cristele Chevalier, Marine Vandenberghe, Marc Pagano, Ian Pellet, Christel Pinazo, et al.. Investigation of dynamic change in microplastics vertical distribution patterns: The seasonal effect on vertical distribution. Marine Pollution Bulletin, 2023, 189, pp.114674. 10.1016/j.marpolbul.2023.114674 . hal-04266164

HAL Id: hal-04266164
https://hal.science/hal-04266164v1

Submitted on 31 Oct 2023

HAL is a multi-disciplinary open access archive for the deposit and dissemination of scientific research documents, whether they are published or not. The documents may come from teaching and research institutions in France or abroad, or from public or private research centers.

L'archive ouverte pluridisciplinaire **HAL**, est destinée au dépôt et à la diffusion de documents scientifiques de niveau recherche, publiés ou non, émanant des établissements d'enseignement et de recherche français ou étrangers, des laboratoires publics ou privés.

Investigation of dynamic change in microplastics vertical distribution patterns: The seasonal effect on vertical distribution

Cristele Chevalier [a,*], Marine Vandenberghe [b], Marc Pagano [a], Ian Pellet [a], Christel Pinazo [a], Javier A. Tesán Onrubia [a], Loïc Guilloux [a], Francois Carlotti [a]

[a] Aix Marseille Univ., Université de Toulon, CNRS, IRD, MIO, Marseille, France
[b] Laboratory of Oceanology and Geosciences, France

Keywords:
Microplastics
MPs surface and water column distribution
1D transport modelling
Turbulence
Settling velocity
Mediterranean Sea

A B S T R A C T

This paper analyzes the variability of microplastics vertical distributions in the oceanic water column. Data were obtained from targeted sampling in the Bay of Marseille (France) and from a numerical simulation forced by realistic physical forcings. By fitting model and in-situ data in a simplified vertical dimension, three microplastics classes may be deduced: settling, buoyant and winter neutrally-buoyant microplastics. Buoyant microplastics are mainly concentrated at the surface but they can be mixed throughout the whole water column during episodes with strong winds and no water stratification, inducing an implicit underestimation of buoyant microplastics in surface sampling. Almost symmetrical to the distribution of buoyant microplastics, settling microplastics are mainly found at the bottom but they can sometimes reach the surface under the mixing conditions cited above. They could thus contribute to surface sampling. Winter neutrally-buoyant microplastics are more homogenously mixed during the winter but are under the stratified layers during summer.

1. Introduction

Due to their long life-span (thousands of years, Barnes et al., 2009), plastics have a long-term impact on ecosystems. Plastics debris break down into smaller pieces in the environment through various physical, chemical or biological processes (Barnes et al., 2009; Brandon et al., 2016; Biber et al., 2019), and this process results in small-sized plastics, referred to as meso- (>5 mm), micro- (1 μm – 5 mm) and nano- (<1 μm) plastics. Washed away by rain and carried by wind, rivers and streams, oceans become their main final destination. These particles then constitute a threat at the base of the oceanic pelagic food chains. They may represent potential false prey for planktivorous organisms (Jambeck et al., 2015; Lehtiniemi et al., 2018) when they reach a size of the same order as planktonic organisms at the base of pelagic food webs. Then, knowing the microplastics (MPs) distribution from surface to bottom is a key issue in order to understand their impact on the ecosystem.

The spatial distribution of MPs at sea is the subject of an extensive corpus of literature which has mainly focused on horizontal accumulations at the sea surface and/or at the sea floor in coastal areas. In general, these studies show MPs distributions are characterized by a high temporal and spatial variability for a wide spectrum of MPs size and density (e.g. Tsiaras et al., 2022). However, little is known about the presence of PMs in the intermediate layers because the vertical distribution within the water column has been rarely studied. Sampling of MPs is mainly carried out at the surface and bottom interfaces. The position of MPs within the water column is often considered to be a transient state, with much lower concentrations than at the surface and bottom interfaces. In-situ MPs sampling at different levels in the water column to observe water column MPs distribution pattern has rarely been done, and the profiles of vertical MPs have consequently seldom been described (Kooi et al., 2016; Lenaker et al., 2019). However, neglecting the MPs distributed through the water column may lead to an underestimation of plastics concentrations in the oceanic realm (Kukulka et al., 2012; Hidalgo-Ruz et al., 2012; Kooi et al., 2016; Lenaker et al., 2019; Van Sebille et al., 2020; Defontaine et al., 2020). Moreover, knowing the vertical MPs distribution is critical for understanding biota/MPs interactions. For instance, predation by planktivorous organisms mainly occurs in layers of high plankton density. High concentrations of MPs in these layers, could lead to a higher ingestion of microplastics by these predators and become an issue.

Therefore, assessing vertical MPs distribution from surface to bottom

is a key issue for understanding the MPs impact on the biota functioning but it remains a major challenge to achieve this experimentally. Some studies have attempted to describe the key processes and parameters driving MPs distribution within the water column. Their vertical patterns of distribution are largely due to MPs intrinsic characteristics in link with their size, shape and density: Low density polymers (such as polypropylene and polyethylene, density below 1 $kg.l^{-1}$) are found mainly at the sea surface (25 % and 42 %, respectively), but much less in the water column (3 % and 2 % in the deep-sea, respectively) (Erni-Cassola et al., 2019). Denser polymers (such as polyesters and acrylics, density above 2 $kg.l^{-1}$) are predominant in deep-sea locations (77 %) and have low concentrations at the sea surface (5 %) (Erni-Cassola et al., 2019). However, the MPs size, shape and density are altered by chemical and biological factors such as fragmentation or biofouling and they vary with time and environmental conditions (Kooi et al., 2016; Nguyen et al., 2020) inducing a possible change in the MPs vertical distribution. MPs distribution in the water column is also dependent on external forcings, primarily the marine vertical dynamics including vertical velocity and vertical turbulence driven by wind stress (Li et al., 2018), as well as the stratification and the velocity gradient. MPs horizontal transport is linked to the hydrodynamics of the layer where they accumulate. For the buoyant MPs it is driven by the surface currents in relation with the wind, the Ekman profile, and the Stokes drift (Lebreton et al., 2012; Onink et al., 2019; Van Sebille et al., 2019), whereas for settling MPs it is driven the dynamics of the bottom boundary layer. Besides, the displacement of any MPs suspended in the intermediate waters between surface and bottom depends on the 3D dynamics in the water column.

Many models describe the transport of buoyant MPs in surface water, using Lagrangian dispersion models (Eriksen et al., 2014; Van Sebille et al., 2015; Maximenko et al., 2012; Lebreton et al., 2012), but only a few of them (e.g. Daily and Hoffman, 2020; Defontaine et al., 2020) have taken into account the vertical advection processes (sinking or rising) as well as the turbulent diffusivity. However, modelling the vertical MPs displacement in the water column may improve the spatial quantification of MPs (Van Sebille et al., 2020; Kooi et al., 2016). It can also help in estimating the quantity of MPs in the marine layer where plankton is present. Vertical modelling studies are required to better understand the impact on the vertical distribution of various forcings such as wind stress, current velocity gradients and stratification on any types (buoyant, drifting, settling) of MPs.

In this context, the aim of the present study is to assess how the climatic context (namely seasonal variation of temperature and wind events) can impact the vertical distribution of MPs in coastal waters. For this purpose, we focus on MPs vertical distribution from surface to bottom and their variability in a coastal area. We have combined field observations and a one-dimension vertical (1DV) model, taking as example atmospheric and hydrographical conditions at the SOLEMIO station (Bay of Marseille, France) and making two major assumptions:

- Assumptions regarding the microplastics categories: we consider that all MPs are distributed within a limited number of idealized MPs classes, each of them with a unique density and a unique size of MPs. These characteristics are not altered by chemical and biological factors and do not vary with time (A1); In addition, MPs vertical velocity in each class comes from an empirical mathematical representation (Ahrens law, see Material and Methods section).
- Assumptions regarding the processes in a 1DV context: we assume a horizontal-homogenous area and a horizontal water circulation (A2). This assumption enables us to focus on the MPs vertical distribution and to highlight the main forcings inducing variability of this MPs vertical distribution. However, the turbulence profile come from 3D hydrodynamics model in which the main physical forcings are considered.

Hence, in the present article, after describing the sampling and numerical model, we first analyzed the vertical MPs distribution patterns at two different dates issued from dedicated horizontal MPs sampling and deduced MPs characteristics thanks 1DV model. Then, we present a one-year 1DV simulation of MPs vertical distribution considering the turbulent viscosity of the seawater obtained from a 3D hydrodynamic model, and for different MPs characteristics. Next, we analyze the main forcing constraining the change in dynamic vertical distribution. Finally, we investigate the dynamic changes of MPs vertical distribution over the simulated year. This assessment of the vertical distribution in relation with weather conditions could help to improve the estimation of the whole MPs stock based on traditional surface sampling.

2. Material and methods

2.1. Study site

The monitoring station, located at the SOLEMIO station (43:14:30 N 05:17:30 E), part of the French national program SOMLIT, has been extensively observed. It is located in the Bay of Marseille at 55 m depth, in the eastern part of the Gulf of Lion in the North-Western Mediterranean Sea (Fig. 1). The hydrodynamics in this area is complex and highly variable (Petrenko et al., 2005), but well documented and modelled. It is influenced by several environmental forcings such as freshwater inputs, wind forcing and the general eddies circulation (Millet et al., 2018), including the Mediterranean Northern Current. The north-northwesterly (Mistral wind) or southeasterly winds (maritime winds) are one of the main forcings of this circulation. They can quickly increase in speed up to 8 $m.s^{-1}$ and also disappear abruptly. These wind variations generate transitional circulation features. The bay is also influenced by the Mediterranean Northern Current (Millot, 1990, 1992) which flows along the continental slope bordering the Gulf of Lion and can intrude on the continental shelf (Petrenko et al., 2005; Estournel et al., 2003). The Bay of Marseille is in addition regularly impacted by Rhone River inputs, a major Mediterranean river, as a significant source of freshwater and also of MPs (Schmidt et al., 2018, 2019). In addition, coastal industries and the quantity of sewage discharge are typical of large industrial coastal Mediterranean cities. The flow velocity around the SOLEMIO station is mainly horizontal with a retention and recruitment area (A2).

2.2. MPs field sampling and processing

MPs samples were collected on February 3rd and 10 th 2020 at the SOLEMIO station on board the R/V Antedon II, using a Hydrobios multinet (0.25 m^2 aperture, five 200 µm mesh closure nets) towed horizontally at different depths (Table 1), until filtered volume for each net reaches 50 or 80 m^3 depending on plankton load. In addition, a Manta tow net (0.075 m^2 opening, 330 µm mesh-size net) was towed at the sea surface during 10 min at a speed of about 2–2.2 knots to reach a filtration volume near of 50m^3. Temperature, salinity, and water density profiles, obtained by a Conductivity Temperature Depth (CTD), and fluorescence profile, by a fluorometer, were also measured at each date.

Multinet samples were sieved through a 330 µm mesh-size to count the MPs above this size. First, plankton samples were fractionated in equal sub-samples using a Motoda box and all the sub-samples were then observed using a binocular dissecting microscope and a Dolfuss chamber. MPs were visually extracted based on their forms and colors, with the help of dissecting forceps and a micropipette, and then isolated in small tubes.

2.3. The model

2.3.1. Transport equation and vertical discretization

In the present study, we assume that MPs displacement is only in the vertical dimension (1DV, A2). Therefore, we consider that the MPs concentrations through the water column only depend on the vertical

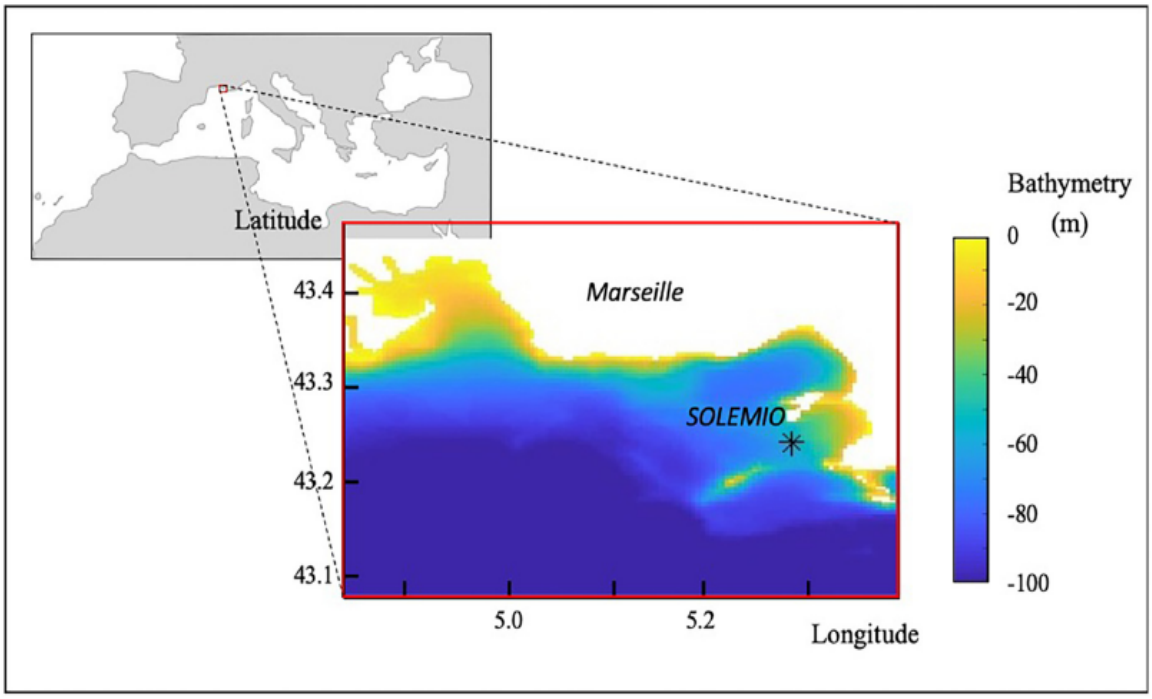

Fig. 1. Bathymetry of the Bay of Marseille and position of the sampling station: SOLEMIO.

Table 1
Metadata for the two sampling dates at the SOLEMIO station.

Date (dd.mm.yyyy)	Wind at 10 m high ($m.s^{-1}$)	Type of net and mesh size	Depth (m)	Filtered Volume (m^{3})
03.02.2020	10.0 (force 4 in the Beaufort scale)	Manta – 330 µm	0 (surface)	48.3
		Multinet – 200 µm	25	80
			35	80
		Observed fraction >330 µm	45	80
			50	80
10.02.2020	7.7 (force 3 in the Beaufort scale)	Multinet – 200 µm	1	50
			10	50
		Observed fraction >330 µm	15	50
			40	50

velocity and diffusivity (i.e., we hypothesize that concentrations are horizontally homogenous). Moreover, we assume that the MPs vertical velocity is much higher than the water vertical velocity. Then, the local MPs distribution (C) depends on vertical turbulent diffusivity (K_z) and on the velocity reached by the MPs at equilibrium which is referred to as "terminal MPs velocity" (w_s) by Kooi et al. (2016). This velocity, also referred to as settling or rising vertical velocity, is in function of depth (z) and time (t).

$$\frac{\partial C(z,t)}{\partial t} = \frac{\partial K_z(z,t)\,\partial C(z,t)}{\partial z^2} + w_s(z,t)\,\frac{\partial C(z,t)}{\partial z} \tag{1a}$$

The water column is discretized with a finite volume model, and we use a 1-D up-wind model (Enders et al., 2015) to avoid 1-D centered model oscillation. The discretization is taken fine enough to limit the diffusion problem of the up-wind model (2000 meshes of 3 cm). Integrated water-column MPs abundance is considered constant over time, which means that there is no addition and no loss of MPs during simulations. The model is initialized with a uniform MPs distribution. Then, MPs move from mesh to mesh starting from their initial location. Incoming and outgoing fluxes (inflows and outflows) in each mesh depend on the turbulent viscosity and on local MPs velocities. Three main MPs behaviors may be observed: rising, or settling, or remaining within the water column, depending on terminal velocity; a low velocity leads to well-distributed MPs in the water column while a high terminal velocity concentrates MPs at the surface or at the bottom. The turbulence leads MPs dispersion: Hence, strong turbulence tends to homogenize the water column.

With Q(t), the MPs abundance within the water column which depend on time only and $\chi_i(t, z)$, the vertical distribution that depends on time and depth, defined as:

$$C(t,z) = Q(t)\,\chi(t,z) \text{ with. } \int_{-H}^{0} \chi(t,z)\,dz = 1$$ Where H is the total depth of the water column. Thus Eq. (1a) becomes:

$$\frac{\partial \chi(z,t)}{\partial t} = \frac{\partial K_z(z,t)\,\partial \chi(z,t)}{\partial z^2} + w_s(z,t)\,\frac{\partial \chi(z,t)}{\partial z} \tag{1b}$$

2.3.2. MPs terminal velocity

The terminal velocity of a given particle depends on its characteristics (size, form and density), and on the water density. Small particles in suspension have been studied for many years, particularly the settling velocity of sand grains and mud in sedimentology. Many empirical formulations of the terminal velocity of all types of particles have been proposed, and most of them have been calibrated with parameter values obtained from experimental velocity measurement. However, still very few theoretical studies have proposed dedicated formulations of terminal velocity for MPs in water (Khatmullina and Isachenko, 2017, Choi et al., 2022). In their article, Khatmullina et al. tested the already existing formulation of marine sedimentology terminal velocity on MPs. By means of a set of laboratory experiments with MPs, they found that the Ahrens' (2000) formula established with data from Hallermeier (1980) and driven with quartz particles presented the best fit for poly-caprolactone spherical MPs. In the present study, considering spherical MPs, we will use the Ahrens formula to calculate MPs terminal velocity, as this mathematical formulation is continuous and derivable, thereby avoiding potential modelling problems.

$$w_s = \delta\frac{\nu}{d}\left(A_l D_*^{3} + A_t\sqrt{D_*^{3}}\right) \tag{2}$$

with:

- $\delta = 1$ or -1, the sign of MPs velocity: positive if the MPs is denser than the water ($\rho_p/\rho_w > 1$); negative if not;
- A_l and A_t two calibration coefficients:

$$A_l = 0.055\ tanh\left[12{D_*}^{3-0.59} exp\left(-0.0004{D_*}^3\right)\right]$$

$$A_t = 1.06\ tanh\left[0.016{D_*}^{3^{0.50}} exp\left(-\frac{120}{{D_*}^3}\right)\right]$$

$D_* = \sqrt[3]{\frac{g\left|\rho_p/\rho_w - 1\right|}{\nu^2}}d$, the Archimedes buoyancy index

- ρ_w *and* ρ_p, respectively water and MPs densities
- ν, kinematic viscosity of sea water
- g, the acceleration due to gravity
- d, the MPs diameter

Then, the three main MPs behaviors (rising or settling or remaining) observed within the water column depend on the MPs density relatively to water density. Hence, for a same MPs size, if MPs density is close to the water density, the MPs velocity is low and MPs well-distributed MPs in the water column; on the opposite, if the MPs density is widely different from the water density, the terminal velocity is high, and MPs concentrated at the interface.

2.3.3. Methodology of validation – indices of model robustness

Analytical solutions are deduced in stationary situation assuming water density, velocity and turbulent diffusivity are respectively constant:

$$C = C_a e^{-\frac{w_s}{K_z}z} \tag{3}$$

with C_a, the concentration at the surface when $z = 0$.

The modelled vertical MPs distribution is calculated from the initial situation until a stationary solution is reached when vertical turbulent diffusion balance MPs terminal velocities in the Eqs. (1a) and (1b) and the concentration become constant in time. Then, this solution is compared to analytical solution in steady situation (for validation) or to field data (for retrieving MPs density) using RMSE (Eq. (4)) as an index to estimate the similarities.

$$RMSE = \sqrt{\frac{\sum_i^n \left(C_i - C_{modelled,i}\right)^2}{n}} \tag{4}$$

With C_i and $C_{modelled,i}$ respectively MPs reference and modelled concentrations at mesh *i*; n, number of meshes (n = L/dx). In function of aims, the MPs reference concentration is the field concentration or the analytical concentration.

This index is used to validate the model or to find the MPs density. The RMSE depends on the concentration in the water column. To avoid this bias, we also calculate the relative error, which is the ratio between the RMSE and the maximum concentration in the water column.

2.3.4. Choice of MPs

In our simulations, a single size of MPs will be considered and set to 350 μm, an average size of isolated MPs from our field study, but the MPs density varies with simulations leading to different MPs behaviors. Hence, different classes of MPs will be considered, and each class is characterized by a density value, remaining constant in time (A1). However, although we consider that the characteristics of MPs (shape, size, and density) are specific of each class of MPs and constant spatially and temporally, the terminal velocity varies over time and vertical location with the water density, as presented in *Supplementary Materials* (Fig. 1). We also assume no interaction with other particles.

2.3.5. Realistic simulations data

To perform realistic situations, turbulence profiles at the SOLEMIO station were extracted from the simulation results of the Bay of Marseille MARS3D-RHOMA coupled hydrodynamic-biogeochemical model (Pairaud et al., 2011; Fraysse et al., 2013). Based on the three-dimensional MARS3D model (3D hydrodynamic Model for Applications at regional Scale, IFREMER, Lazure and Dumas, 2008), the high resolution MARS3D-RHOMA configuration was applied and validated to simulate the oceanic circulation off Marseille (Fraysse et al., 2014; Ross et al., 2016; Millet et al., 2018; Schmidt et al., 2019), with a horizontal resolution of 400 m and 30 sigma vertical levels. The time step was fixed at 30 s. Realistic atmospheric conditions obtained from the WRF regional meteorological model (Yohia, 2016), the average daily inputs of the Rhône River and the hydrodynamic forcings calculated by the large scale regional MARS3D-MENOR configuration (1.2 km resolution) (Nicolle et al., 2009), were imposed at the open boundaries. Viscosity and diffusivity coefficients related to vertical mixing are given by the turbulence closure scheme of Gaspar et al. (1990). At the bottom, they mainly vary with the bottom shear stress, while at the surface, they are mostly dependent on the wind intensity with a correlation of about 0.83 between wind intensity and the maximum of vertical turbulent diffusivity in the upper layer during the simulation over one year used in this article.

2.4. Retrieval of mean MPs density using field data and vertical transport modelling

We first assume that the total quantity of MPs in the water column (Q) is divided in a set of N classes (i), each corresponding to a representative constant MP density. Then, Q is the sum of MP quantities of each class (Qi), that may vary with time. The interaction between classes is neglected and the concentration of each class (Ci) at a given depth (z_k) follows Eq. (1b).

For the N considered classes of MPs, all possible combinations of density classes are tested, with a "reasonable" accuracy of ± 0.1 kg/m^3. Then, for MPs density ranging from 1025 kg/m^3 to 1035 k/m^3, 100^N possible set of classes are tested.

For each MP class *i*, we obtain, by using Eq. (1b), the numerical MPs relative vertical distribution profiles for sampling days 1 and 2 (February 3rd and February 10 th) : $\chi_i^1(z)$ and $\chi_i^2(z)$. These profiles only depend on MPs density and water characteristics and do not depend on the MPs abundance.

The cumulated MPs abundances within a set of N classes, for the sampling days 1 and 2 is then adjusted by fitting the corresponding numerical concentrations C_k^1 and C_k^2 at depth z_k with the experimental concentrations $\widehat{C_k^1}$ and $\widehat{C_k^2}$ of the same sampling days at level *k*, knowing numerical concentrations C_k^1 and C_k^2 are given by:

$$C_k^1 = \sum_{i=1}^{N}\left(Q_i^1\,\chi_i^1(z_k)\right) \text{ and } C_k^2 = \sum_{i=1}^{N}\left(Q_i^2\,\chi_i^2(z_k)\right) \tag{5}$$

Where Q_i^1 and Q_i^2 are the are the MP quantities of the class i for the sampling days 1 and 2.

z_k represents the sampling depth for the sample k; k varies between 1 and 5 for the first sampling day and between 1 and 4 for the second sampling day.

This fitting was performed by least square method. The RMSE was also calculated for each set of classes and the set that minimizes the RMSE was selected. Thus, for a given number of classes, we were able to find the set of classes (with density, total abundance for day 1 and for day 2 of each class) that minimizes the discrepancy between in-situ and numerical data.

Note that for each MPs class, we look for 3 unknowns (the MPs density which gives the MPs distribution for each sampling day, the total abundance on February 3rd and February 10th). Thus, for N classes and 2 sampling days, we have 3*N unknowns. In the same way, each sampling gives rise to one equation (the linear combination of MPs concentration of each class). Then, 5 sampling depths on February 3rd and 4 sampling depth on February 10 th (Table 1) induce 9 samplings and a system of 9 equations which explicit the MPs total concentration in function of MPs concentration of each class. Hence, with such a total of 9 sampling depth for two days, it is possible to discriminate up to three MPs classes.

By testing all configurations of density classes (1, 2 or 3 classes), we retrieved the density values which induce the best fit between MPs simulated distributions and observed distributions at the two sampling days (February 3rd and 10th).

2.5. Simulations

Three main numerical experiments have been done:

- Preliminary simulations for validating the vertical transport model and to study the sensitivity to mesh size for different levels of turbulence. These simulations are done in transitional state from the initial condition, but we have waited for steady state to compare with analytical solution.
- A first set of simulations to estimate the density values for MPs classes. As for the validating test case, the simulation begins from the initial condition, but we waited for steady state to compare these distributions with data to find the density values with the best fit.
- A second set of simulations to estimate how the vertical MPs distribution varies in time over one year, assuming a constant water-column MPs abundance and constant density value. In accordance with in-situ data analysis, three MPs classes are investigated: buoyant, settling and winter neutrally-buoyant (MPs size diameter set to 350 μm).

  We also assume no change with time of integrated water-column MPs abundance, no entry or loss and no fragmentation, aggregation, or interaction with other particles.

3. Results

3.1. Validation of vertical transport model and sensitivity to mesh size

The model is validated by comparing the solution in stationary situation with an analytical calculation in the case of a constant turbulent diffusion (see Eqs. (1a) and (1b)). The relative error (RMSE) ranges from 10^{-1} to 10^{-3} % (Fig. 2). As expected, it depends on the discretization but also on the vertical turbulent diffusivity. It decreases with the number of meshes and it is inversely proportional to the vertical turbulent diffusivity when the mesh discretization is enough to well represent the distribution. From a value of 500 meshes, the error remains below 0.1 %.

The initial conditions of MPs distributions in the water column do not affect the final steady MPs vertical distribution. However, it can reduce or increase the time to reach this steady MPs vertical distribution.

3.2. Data

3.2.1. Environmental data

CTD salinity and temperature profiles through the water column on the two sampling days (Fig. 3a and b) show warmer and overall saltier seawater on February 3rd than on February 10th. The temperature increases from 13.6 °C (and 13.6 °C, respectively) at the surface to about 14.4 °C (and 14 °C) at 20 m depth, then it decreases to 14 °C (and 13.8 °C) at the bottom. The salinity globally increases from 37.4 (and 37.7) at the surface to about 38.45 (and 38.4) at the bottom. As a result, the density profiles of the two days vary from 1028.1 to 1028.7 and from 1028.25 to 1028.7 (Fig. 3c). A surface layer, characterized by a salinity and a temperature weaker, is observed until 5 m on February 3rd and 25–30 m on February 10th. This layer reveals a significant Rhône River diluted water intrusion in the Bay of Marseille and is well reproduced by the model (*Supplementary Materials*, Fig. 2). Although, the real intrusion on February 10th is deeper than the one modelled, the two general profiles were qualitatively well reproduced by the model, namely the lower temperature values measured in the water column on February 10th in comparison with February 3rd, and the salinity under the intrusion layer which is almost the same for the two profiles.

The vertical turbulent diffusivity profile at the SOLEMIO station (Fig. 3f) is calculated by the MARS3D model. The February 3rd vertical diffusivity is characterized by two layers of higher values within the surface and bottom layer, respectively to 10^{-2} $m^2.s^{-1}$ at 6 m under the surface and $0.5.10^{-2}$ at 5 m above the bottom. The increase of the diffusivity in the surface layer is mainly driven by the wind mixing, whereas near the floor, it is probably the consequence of a sheared bottom current. On February 3rd, this bottom current seems to be linked to the upwelling driven by wind conditions as simulated by the hydrodynamic model. On February 10th 2020, vertical diffusivity is about 10^{-3} $m^2.s^{-1}$ in the water column and $2\ 10^{-3}$ $m^2.s^{-1}$ at the upper layer, lower than on February 3rd, consistently with the weaker wind.

3.2.2. Field MPs distributions

The vertical MPs distribution (Table 2) observed on February 10th is

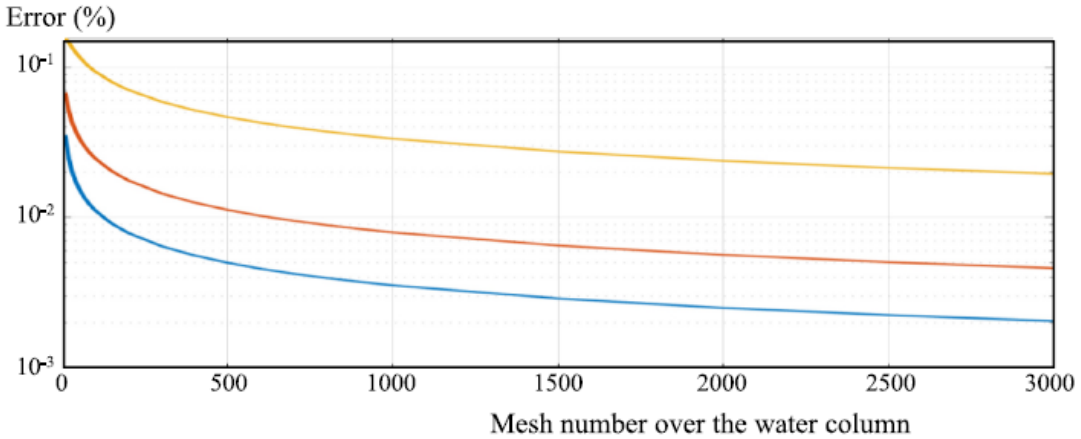

Fig. 2. RMSE relative error (ratio between RMSE and maximum of concentration in each profile) as a function of mesh number and vertical diffusivity. Colour lines indicate the vertical diffusivity value: blue line, 0.01 $m^2.s^{-1}$; red line, 0,001 $m^2.s^{-1}$ and orange line 0.0001 $m^2.s^{-1}$.

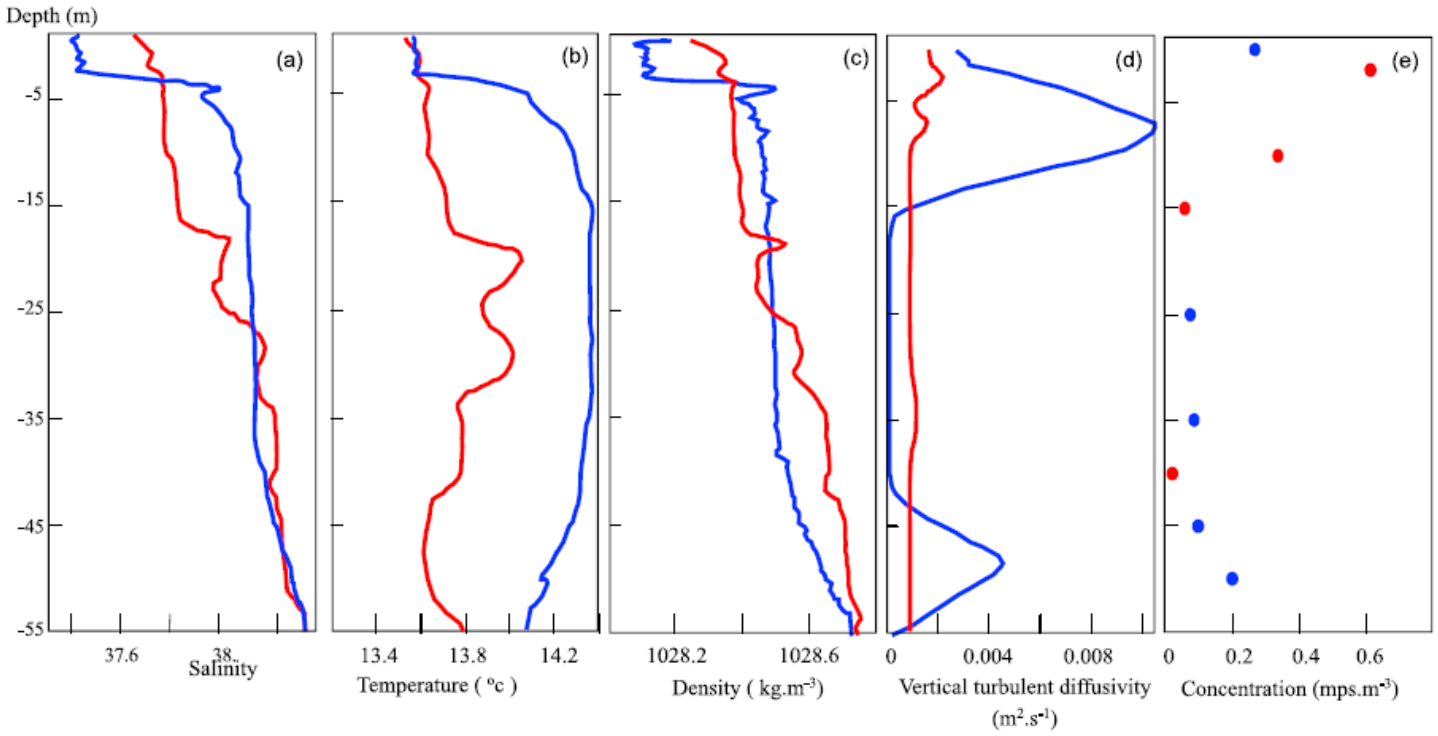

Fig. 3. Vertical profiles of (a) CTD temperature, (b) CTD salinity, (c) CTD density, (d) modelled turbulent diffusivity and (e) MPs vertical distribution, on February 3rd 2020 (blue lines and blue markers) and February 10th 2020 (red lines and red markers).

Table 2
MPs distribution for the two sampling dates at the SOLEMIO station.

Date (dd.mm.yyyy)	Depth (m)	MPs concentration (mps/m^3) from sampling	MPs concentration (mps/m^3) from simulation	Buoyant MPs concentration (mps/m^3) from simulation	Neutral MPs concentration (mps/m^3) from simulation	Settling MPs concentration (mps/m^3) from simulation
03.02.2020	0 (surface)	0.27	0.27	0.20	0.07	0
	25	0.08	0.08	0	0.08	0
	35	0.09	0.08	0	0.08	0
	45	0.1	0.13	0	0.07	0.06
	50	0.2	0.19	0	0.07	0.12
	Water column MPs abundance (mps/m^2)	*7.24*	*9.13*	*2.96*	*3.99*	*2.19*
10.02.2020	1	0.62	0.62	0.60	0.02	0
	10	0.34	0.34	0.32	0.02	0
	15	0.06	0.04	0.00	0.03	0
	40	0.02	0.04	0.00	0.04	0
	Water column MPs abundance (mps/m^2)	*7.92*	*7.40*	*5.65*	*1.75*	*0*

characterized by a high concentration close to the sea surface (0.6 MPs.m^{-3}), which vanishes with depth to nearly 0 at 40 m depth (Fig. 3e). This distribution profile looks like a theoretical vertical distribution of buoyant MPs. In contrast, the vertical MPs distribution observed on February 3rd (Table 2) reaches two local maxima, both near the interfaces (0.30 MPs.m^{-3} at the surface layer and 0.20 MPs.m^{-3} at the bottom layer). This latter distribution seems to contain a mixing of MPs with different densities.

3.3. MPs class density

To be consistent with the winter field observations on February 3rd (Fig. 4a) and 10th (Fig. 4b), three configurations of MPs class densities were tested, with one, two and three classes of different densities. The best RMSE (mean difference model/field data) was obtained with 3 MPs density classes: 1) one class of buoyant MPs with density lower than water density. Their density is equal to 1026.6 kg.m^{-3}; they tend to float during the sampling environmental conditions (without mixing); 2) one class of winter neutrally-buoyant density MPs with density close to water density measured during sampling. Their density is equal to 1028.6 kg.m^{-3}, they tend to remain within the water column in sampling environmental conditions (without mixing); and 3) a last class of settling MPs with density equal to 1033.5 kg.m^{-3}. Their density is higher than the one of water and they tend to settle in sampling environmental conditions (without mixing). With these three MPs classes, the RMSE value is 2 %: an error of about 0.3 % for the sampling of February 10th, and 4.3 % compared to the field distribution of the sampling of February 3rd. Then, we can analyze the MPs composition and distribution within the water column (Table 2).

The simulated MPs concentrations on February 3rd (Fig. 4a) deliver 3.0 MPs.m^{-2} of buoyant MPs, 4.0 MPs.m^{-2} of winter neutrally-buoyant MPs and 2.2 MPs.m^{-2} of settling MPs (respectively 32 %, 44 %, and 24 % of the total water-column MPs abundance). Buoyant MPs are concentrated in the 20 m-surface layer, winter neutrally-buoyant density MPs

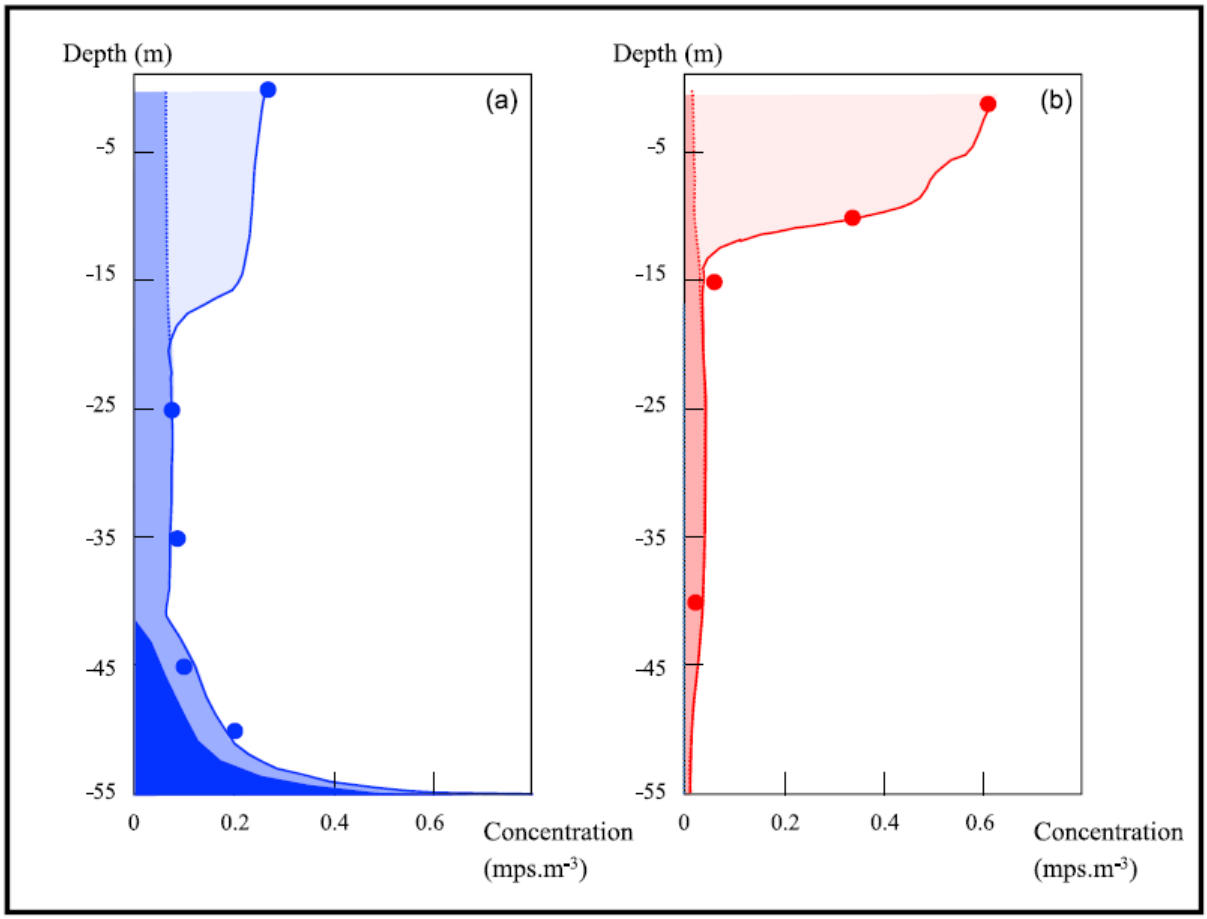

Fig. 4. Measured (dots) and modelled MPs distributions (cumulated surfaces) on February 3rd 2020(a), and on February 10th, 2020 (b). Contribution od the three MPs classes to the simulated profiles: Buoyant MPs (density of 1026.6 kg.m^{-3}) light colored surface; Settling MPs (density of 1033.5 kg.m^{-3}) dark colored surface; winter neutrally-buoyant density MPs (density of 1028.6 kg.m^{-3}).

are quite homogeneously distributed in the water column, and the settling MPs are concentrated in the 15 m-bottom layer. The total water-column simulated MPs abundance (9.13 MPs.m^{-2}) is slightly higher than that (7.24 MPs.m^{-2}) calculated by integrating observed concentrations in the water column based on the trapezoidal integration method. This difference is mainly due to the simulated MPs profile in the 17 m upper layer for which no field data are available except at the surface.

On February 10th, the vertical MPs distribution (Fig. 4b) enable us to estimate that buoyant MPs represent about 5.6 MPs.m^{-2} versus 1.8 MPs.m^{-2} for winter neutrally-buoyant density MPs (i.e. respectively 76 % and 24 % of MPs). No simulated settling MPs are found to fit the field MPs profile. The distribution of buoyant MPs is mainly concentrated below the surface layer at the top of the water column (0-15 m), whereas the winter neutrally-buoyant density MPs are distributed quite homogenously on the vertical. The total water-column MPs abundance from simulation (7.4 MPs.m^{-2}) is slightly lower than the one calculated from sampling data (7.9 MPs.m^{-2}).

3.4. One year simulation of the MPs distribution

During the one-year 1DV simulation of buoyant MPs distribution (Fig. 5), the wind (Fig. 5a) fluctuates over time and the water surface stress ranges from 0 to 1.3 N.m^{-2}. The wind is stronger in winter and autumn due to Mistral and east-wind periods, with a mean of about 0.17 N.m^{-2} and lower in spring and summer with a mean of about 0.06 N.m^{-2}. The bottom water density (Fig. 5b) remains quite constant at about 1028.5 kg.m^{-3}, but the surface water density also varies with season. It is close to bottom density in autumn and winter and decreases to 1025.4 kg.m^{-3} with the surface layer heating in spring and summer, inducing a strong stratification in the water column.

Under these conditions, buoyant MPs move in the water column (Fig. 5d). Their vertical distribution decreases quite exponentially from the surface layer, where their concentrations are the highest, towards the bottom. However, these vertical distributions vary with time, namely with wind and stratification. MPs concentrate in the first meters of the water column, when the wind is low and stratification high, such as on May 20th or on July 19th. Inversely, MPs spread throughout the water column when the wind increases and the stratification decreases, sometimes down to the bottom, such as on January 20th or on February 4th). In such cases, MPs could stay trapped in deep layers for a few days (up to 10 days in January). Inversely, during summer, MPs seem to be rarely below 20 m depth, due to high stratification and less wind stress.

The variability of buoyant MPs vertical distribution induces a change in the ratio within the 15 cm upper layer, generally sampled with Manta nets (Fig. 5c). Hence, the part of MPs in the sampled surface layer ranges from <0.5 % of the MPs mixed in the water column (for instance when the wind is strong and stratification low, on January 20 th or February 4th), to 100 % when the MPs are concentrated in the upper layer as on July 19 th, when wind is low and stratification high. We can observe a seasonal variability: the mean value of this ratio over autumn and winter months is about 5 %, whereas it is about 14 % if the ratio is averaged over the spring and summer months.

In contrast, the vertical distribution of settling MPs (Fig. 6a) increases quite exponentially from the surface layer towards the bottom where their concentrations are highest. They are mainly concentrated in

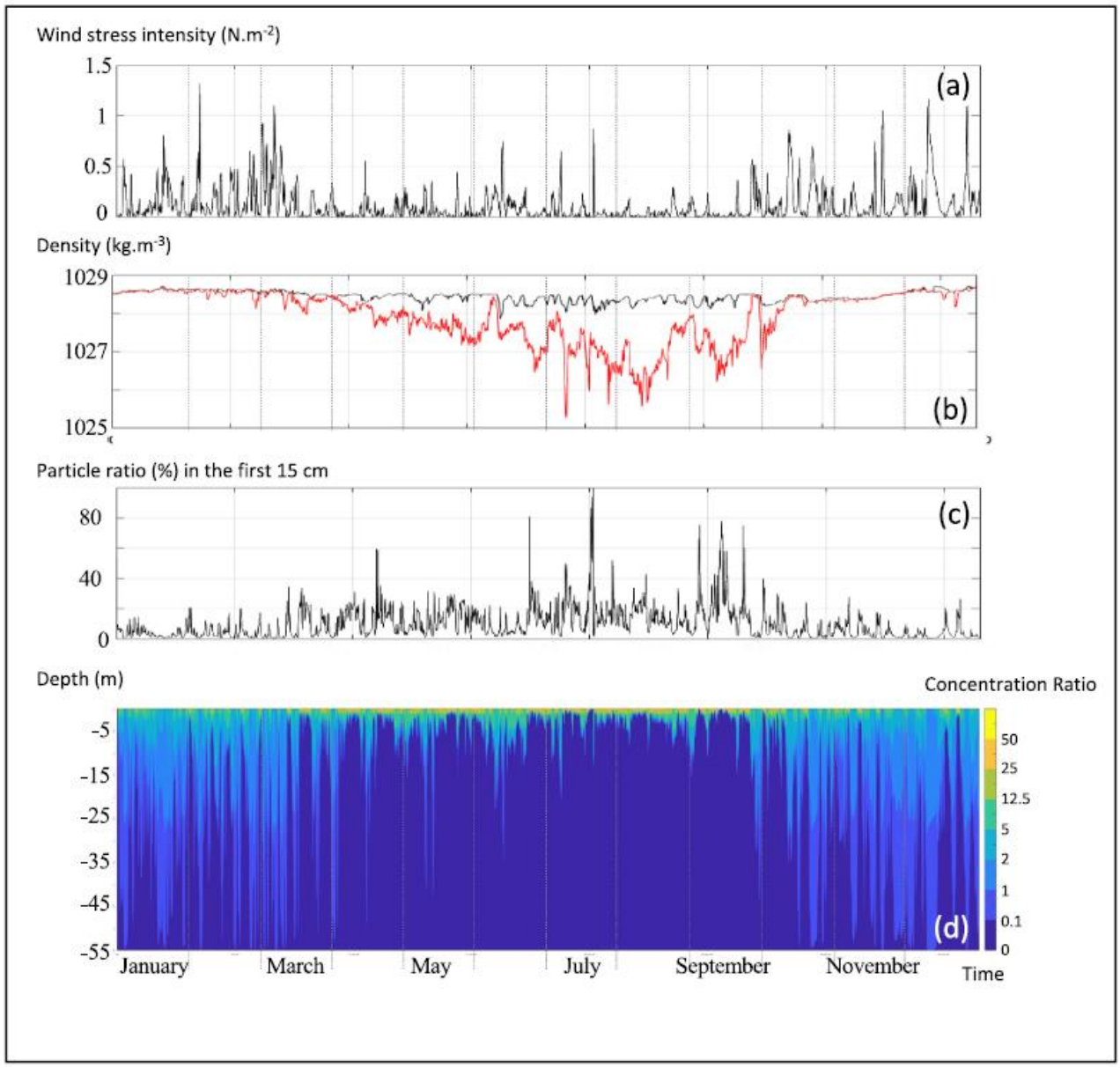

Fig. 5. Variability of the vertical distribution of buoyant MPs over one year
Simulation with (ρ_p = 1026.6 kg.m^{-3} and d = 350 μm) during the year 2012 considering a constant MPs abundance in the water column. (a) Wind stress intensity, (b) water density at the bottom (black line) and at the surface (red line), (c) ratio of MPs in the surface layer (15 cm under the surface) versus the water-column MPs abundance, (d) ratio of MPs concentration versus mean concentration.

the bottom layer, except when vertical diffusivity increases due to wind and bottom shear stress. In this case, settling MPs contribute to MPs collected at the surface and within the water column. In the same way, as the water column density in winter is close to the density of the winter neutrally-buoyant MPs class, winter neutrally-buoyant MPs are homogenously distributed throughout the whole water column in winter (Fig. 6b) and contribute to a constant percentage collected in surface water. During summer, with the water column warming, the water column density decreases inducing winter neutrally-buoyant MPs to become denser than the sea water and settle towards the bottom. Then, we can observe an increase of winter neutrally-buoyant MPs concentration at the bottom, and a decrease of their abundance in surface waters and within the water column. <0.3 % of these MPs reach the surface.

4. Discussion

4.1. Comparison with sampling concentrations of MPs in the Marseille region

The sampling data showed a considerable modification of MPs vertical distribution at the Solemio station between the two sampling dates, only 10 days apart, with: doubling of the surface concentration (from almost 0.3 MPs.m^{-3} to 0.6 MPs.m^{-3}) and decrease of the average water column concentration (from 0.16 MPs.m^{-3} to 0.13 MPs.m^{-3} ie 9.1 MPs.m^{-2} to 7.4 MPs.m^{-2}). This decrease may be due to a horizontal MPs supply on February 3rd, but it could also be due to the burying in the sediment of MPs in suspension in the water column on February 3rd. The numerical model suggests that about 2.2 MPs.m^{-2} of settling MPs were re-injected into the water column, probably due to the wind, on February 3rd, whereas there were no settling MPs during the second sampling day (see Table 2).

Our observations and simulations complete previous data obtained

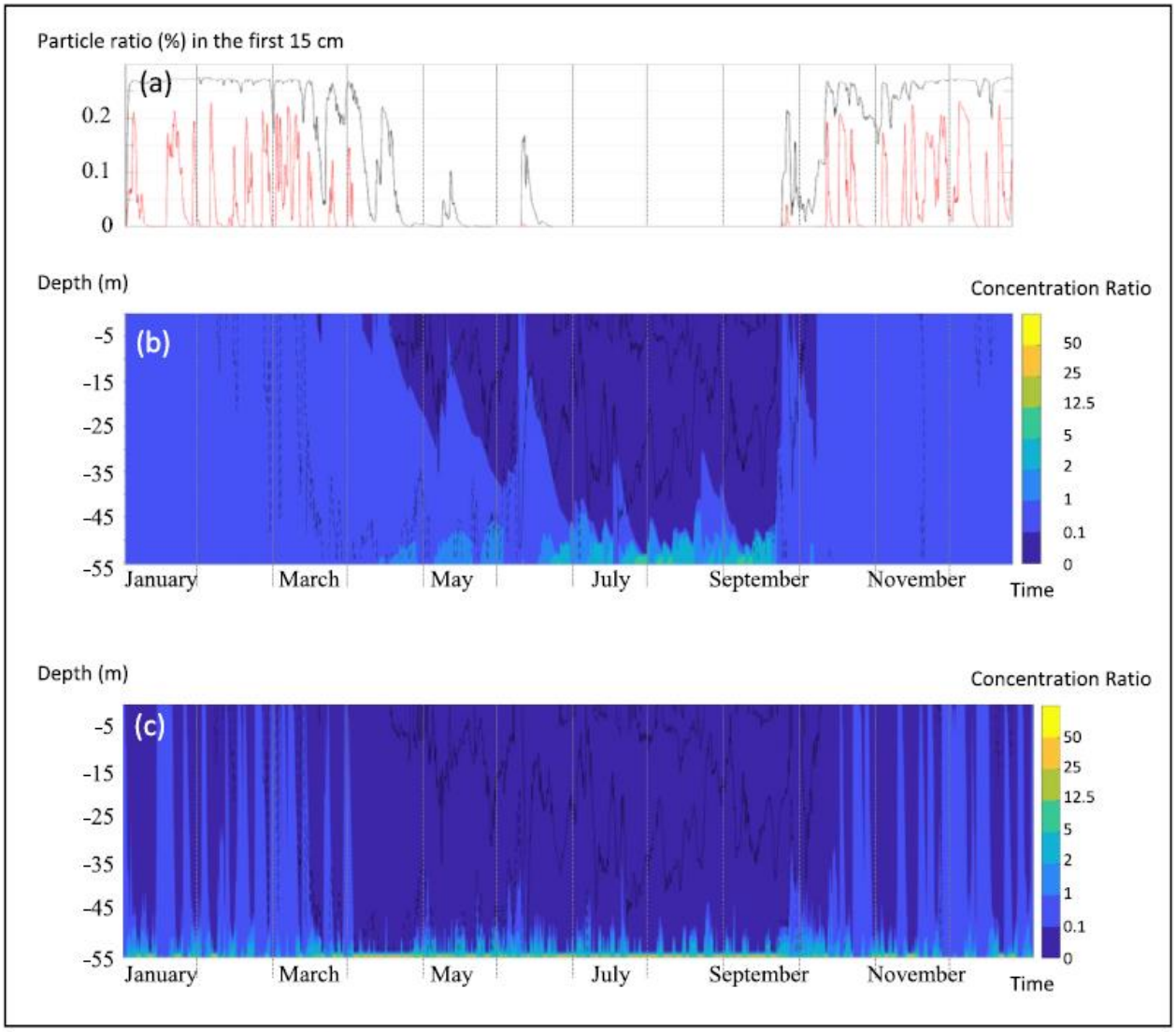

Fig. 6. Variability of the vertical distribution of buoyant MPs over one year
Simulation during the year 2012 considering constant the MPs abundance in the water column. Ratio of MPs concentration versus mean concentration for (a) winter neutrally-buoyant MPs (black line) and for settling MPs (red line) in the surface layer (15 cm under the surface); (b) settling MPs (ρ_p = 1033.5 kg.m^{-3} and d = 350 μm, below) and (c) winter neutrally-buoyant MPs (ρ_p = 1028.6 kg.m^{-3} and d = 350 μm,). (b) and (c) black solid lines indicates the 1027 and 1028 isopycnal, whereas dashed lines indicate the 1028.5 isopycnal.

by different authors around the Bay of Marseille, and generally agree with their estimation. For instance, Lefebvre et al. (2019) found water column integrated concentrations between 0 and 0.7 MPs.m^{-3} in July over 14 stations distributed on the continental shelf of the Gulf of Lion, with an average value of 0.23 MPs.m^{-3} which is slightly higher than our observations. In addition, our observed surface concentration of 0.3 MPs.m^{-3} and of 0.6 MPs.m^{-3} MPs collected with a manta net of 0.15 m depth could extrapolate to a surface MPs abundance of 45. 10^3 MPs.km^{-2} and 93 10^3 MPs.km^{-2}, respectively which is in the range from 6 ·to 100 10^3 MPs.km^{-2} (average 96 10^3 MPs.km^{-2}) observed by Schmidt et al. (2018) in the Bay of Marseille or in the range from 44 ± 23 MPs.km^{-2} in June to 88 ± 80 MPs.km^{-2} described by Kedzierski et al. (2022a, 2022b) in Gulf of Lion.

However, our study also highlights the need to consider the vertical distribution which may strongly increase the estimated MPs quantity, up to factor of 700 on February 10 th and of 2000 on February 3rd.

4.2. Consideration of MPs size and density

The density of microplastics, which are mainly polymers (Andrady, 2017), depends on the monomers used and the type of polymerization. Their properties, including density, can change by the presence of additives such as loads and reinforcements and/or modifiers. Erni-Cassola et al., 2019 estimates that polypropylene polymer is one of the most widely occurring polymers at the sea surface. More specifically, in the Mediterranean Sea, Kedzierski et al. (2022a, 2022b), estimate that polyethylene, and polypropylene are the two major prevalent MPs corresponding to, respectively, 67 %, 21 % of MPs in Gulf of Lion. Their density ranges from 1000 to 1050 kg.m^{-3} for the Blend – polyethylene, from 970 to 1059 kg.m^{-3} for polypropylene polymer with 10–20 % glass fiber or 970–1250 kg.m^{-3} with 10–40 % mineral filled and 10–20 % talc (Crawford and Quinn, 2016). These densities are consistent with the three density classes we obtained in this study by comparing modelling and field data.

However, Lefebvre et al. (2019) estimated the main polymer types encountered in the water column were polyethylene terephthalate (61 %) whose density is 1380 kg.m^{-3} followed by polyamide (31 %) whose density is higher than 1040 kg.m^{-3}, depending on the type of polyamide. This last density is close to the "settling" density (1033.5 kg.m^{-3}), deduced by fitting the simulation with the observed distributions found in the deeper samples on February 3. In contrast, theoretically, taking into account seawater density, high densities of polyethylene

terephthalate seem too high to be found in the whole water column and namely at the surface layer. As clearly shown by Defontaine et al. (2020) using modelling simulation, they would tend to be concentrated in the bottom layer. This could suggest a modification of the MPs density in sea water condition. In the water, the MPs density can vary with different parameters such as the biofilm constitution or aggregation (Kooi et al., 2017, Khatmullina and Chubarenko, 2021, etc.). The density deduced from the distribution during sampling does not take into account the chemical MPs constitution and does not correspond to the exact nature of pure microplastics. However, this density corresponds to the MPs distribution in the in-situ real conditions, considering all the environmental conditions, the form, size, and orientation of MPs (Kooi and Koelmans, 2019, Nguyen et al., 2022,). Hence, the density retrieved by fitting sampling and model is closer to the density in real conditions, including the in-situ complexity and MPs irregularity (shape, porosity, etc.). Therefore, if the density classes could be a consistent representation of the spectrum of MPs densities collected in a study, this fit delivers "apparent density" of MPs which could be a very useful proxy to further model the spatial (vertical and horizontal) MPs distributions.

The main model limitation concerns the number of classes (assumption A1). Due to the number of samplings, we have considered only 3 MPs classes: three densities and one size. In reality, it is more complex and each class may include a continuum of MPs with different density and size. This limitation of one size and one density in each class is compensated by the velocity formulation based on the Archimedes buoyancy index which merge size and density of MPs with fluid characteristics as kinematic viscosity and water density. Hence, in a specific water condition, for the same Archimedes buoyancy index, several size-density couples exist, whose MPs have quite the same terminal velocity. In the same way, the Archimedes buoyancy index changes with environmental conditions, then the terminal velocity also changes with water density variability.

4.3. MPs vertical distribution: Impact of successive wind events and seasonal stratification

As observed by Lenaker et al., 2019, the MPs vertical distributions vary with time and variability depends on the MPs nature (size, density, etc.) as we observe in the one-year 1DV simulation.

The wind intensity is one of the main factors of the variability of MPs distribution. This effect is enhanced for buoyant and settling MPs. As shown by Kukulka et al., 2012, the wind induces a homogenization of vertical MPs distribution. When the wind increases as at the beginning of the year in Fig. 5a (e.g. January 20 th or February 5 th), the buoyant MPs are mixed down to the bottom and the part of MPs located in the surface layer is below 0.5 % (Fig. 5d). Settling MPs show an inverse displacement from the bottom, where they are generally concentrated, to the surface (Fig. 6b). Inversely, in the summertime, when the wind decreases, buoyant MPs are concentrated at the surface layer (Fig. 5c) and settling MPs remain in the bottom layer. The upper layer contains the main part of the buoyant MPs in the water column and the bottom layer contains the main part of the settling MPs in the water column, as observed on July 19 th where all buoyant MPs are in this surface layer and settling MPs at the bottom.

This is also shown with the regression law estimating the part (R) of the buoyant MPs in the upper layer in function of wind (τ) with a good accuracy ($r^2 = 0.78$) (Fig. 7):

$$log\,(R) = -0.6295\,log\,(\tau) - 0.1267 \quad r^2 = 0.78 \tag{5}$$

However, wind is not the only forcing. The MPs distribution also varies with season, and more specifically with water density and stratification. This is particularly visible for winter neutrally-buoyant MPs (Fig. 6a). These MPs spread quite homogenously within the water column during winter, and they are gathered at the bottom during summer. For buoyant or settling MPs, the seasonal impact is also visible: MPs are more concentrated at the interface during spring and summer and more dispersed during autumn and winter, even for the same wind stress (Fig. 5d and 6b). For instance, during high wind intensity (about 0.73

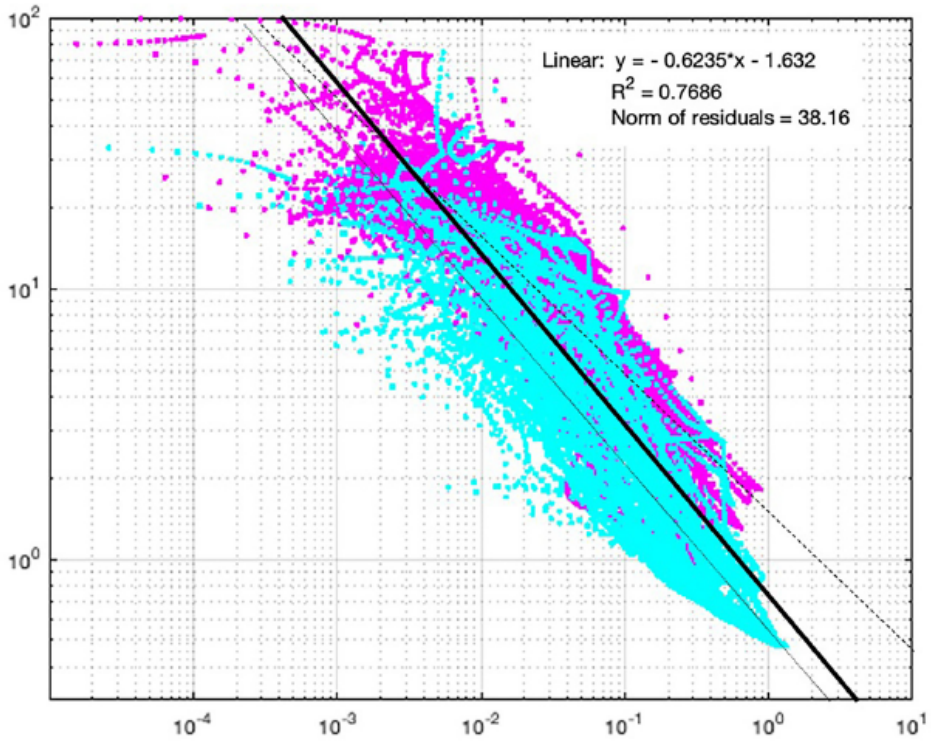

Fig. 7. Ratio of the surface layer (15 cm) MPs abundance versus water-column MPs abundance (%) in function of wind stress at the SOLEMIO station (ρ_p = 1026.6 kg.m^{-3}; d = 350 µm)
Purple points indicates values obtained in spring and summer whereas cyan point indicates values obtained in autumn and winter.

$m^2.\ s^{-1}$), the ratio of surface quantity of buoyant MPs versus water-column buoyant MPs abundance are 1.6 % and 0.2 %, respectively, observed on June 11 th and November 15 th (Fig. 5c). It is the same during no-wind periods, e.g. on January 30 th and June 24 th, the ratio is 20 % in winter versus 33 % in summer for buoyant MPs (Fig. 5c). At the same time, the water density gap between the surface and the bottom is about 1 $kg.m^{-3}$ in summer (1 $kg.m^{-3}$, on June 24 th and 0.9 $kg.m^{-3}$ on June 11 th), and quite null in winter. This underlines the importance of density and stratification for the MPs vertical distribution. The vertical mixing intensity is lower at the thermocline which constitutes a boundary for vertical mixing.

This impact is also visible with the improvement of the fit of the part of the buoyant MPs in the upper layer with a seasonal regression law, (r^2 increase since the mean law). As expected, the ratio of particles located at the surface will be higher during summer than during winter.

$$\text{Winter}: log\,(R) = -0.5956\,log\,(\tau) - 0.2211\ r^2 = 0.80 \quad (6a)$$

$$\text{Summer}: log\,(R) = -0.4909\,log\,(\tau) + 0.2231\ r^2 = 0.79 \quad (6b)$$

Others forcings may modulate the MPs vertical distribution. For instance, the water horizontal bottom circulation induces a bottom shear stress and an increase of the vertical diffusion near the bottom. This induces resuspension and mixing of settling MPs and winter neutrally-buoyant MPs in the bottom Ekman layer. The use of a turbulent diffusivity profile extracted from a realistic 3D hydrodynamic model enables us to take into account the vertical mixing due to all the 3D physical forcings of the Solemio station, to estimate the 1D vertical MPs profile. Furthermore, in contrast to the validation test case, in this one-year simulation the steady state is not reached at each time step. Between two contrasted situations, MPs may need a few hours to reach an equilibrium position and there is a transitional state which can last for a few hours: for instance, when wind stops blowing on July 20 th, (Fig. 5), MPs which are spread out in the water column, progressively reach the surface and are gathered in the surface layer after about 12 h. In contrast, on April 27, when the wind blows, the ratio decreases during about 12 h, which corresponds to the time for changing the water mixing and for the MPs to move until equilibrium.

4.4. *Estimating MPs abundance from surface sampling*

The part of buoyant MPs present in the surface sampling layer versus MPs abundance in the water column varies from 0.5 % to 100 % with a mean of 7.5 % (5 % in autumn and winter and a mean of 14 % in spring and summer, Fig. 5c). Such variability leads to an underestimation of water column MPs based on surface sampling. The regression law proposed in this article can help to correct this underestimation of buoyant MPs by estimating the water column quantity with the surface buoyant MPs sampled. Even if the regression law does not reproduce exactly the time variability, it gives an estimation of the wind impact on the vertical buoyant MPs distribution and enables us to estimate the water-column MPs abundance from the abundance sampled by a net towed at the surface. These data are summarized and extended for all MPs classes, in the abacus depending on season and wind strengths, presented in Table 3 and illustrated in *Supplementary Materials* (Figs. 3, 4 and 5). In the case of wind at Force 0 in the Beaufort Scale, the surface sampling can collect about 76 % of the water column MPs (36 % in autumn and winter and 85 % in spring and summer), whereas only 3 % are sampled (4 % in autumn and winter, 2 % in spring and summer) at Force 5 in the Beaufort Scale and <1 % at Force 9 in the Beaufort Scale (Table 3), the others remaining in the water column.

5. Conclusion

Microplastics is a major issue today and it is crucial to assess and estimate their abundance and distribution in the ocean. However, MPs sampling is the more often performed in the surface layer. Understanding and modelling their vertical distribution is a useful tool to estimate their distribution within the water column as a final step. In this article, we sampled MPs in the water column and analyzed their distribution. Then, we modelled MPs distribution from seawater turbulent diffusivity and MPs features. By fitting field and modelled data on vertical distribution, we also retrieved mean density of three MPs classes. This method allows estimation of the "apparent" density of MPs in real conditions with MPs variability and with their interactions with marine organisms which may also modify their buoyancy (aggregation, fecal pellets, marine snow, etc.) (Coyle et al., 2020). Hence, although it does not reflect the whole of the possible broad density range which might be found, this method gives a rough idea of "apparent" densities of MPs present in the water column. Keeping in mind that the spectrum of MPs shape, size and density is broad, this indicator could be a good alternative to the costly density determination methods. It does precisely reflect the MPs distribution in the water column, including the complexity of MPs density alteration as biofilm, age, etc. Moreover, like the Archimedes buoyancy index, to a certain extent, this term may include the effect of form and size in MPs terminal velocity and then in the MPs vertical distribution. Therefore, with few classes, it could compensate the broad variability of MPs.

Our study also analyzes the variability of MPs vertical distribution over one year considering three MPs classes (buoyant, settling and winter neutrally-buoyant). Then it investigates the wind and water stratification impact on the MPs distribution. It highlights that buoyant MPs tend to remain in the surface layer whereas settling MPs remain in the bottom layer during low-wind days or during high-stratification events. During windy days, a large part of the MPs are drawn into the water column. Stratification decreases this mixing. For instance, it may partially wash out the winter neutrally-buoyant microplastics into the water column from deeper layers in summer conditions.

Finally, our annual simulation suggests that settling microplastics MPs make potentially a very low contribution to surface sample collection, whereas winter neutrally-buoyant MPs impact the concentrations in the water column down to the bottom, namely in winter. Therefore, sampling during no-wind and high-stratification periods should be more representative of the buoyant MPs stock in the water column, whereas surface sampling in windy conditions underestimates

Table 3
Microplastic quantity in the first 15 cm of the water column (in % of the total quantity in the water column) in function of classes and wind (with force in the Beaufort scale) (d = 350 μm).

	Particles	Force 0	Force 1	Force 2	Force 3	Force 4	Force 5	Force 6	Force 7	Force 8
Mean	Buoyant	76 %	33 %	23 %	13 %	6.5 %	3.1 %	1.6 %	1.0 %	0.65 %
	Neutral	4.10^{-2} %	0.07 %	0.1 %	0.2 %	0.15 %	0.18 %	0.23 %	0.23 %	0.28 %
	Settling	0 %	2.10^{-3} %	4.10^{-3} %	0.01 %	0.02 %	0.04 %	0.08 %	0.17 %	0.24 %
Spring and Summer	Buoyant	85 %	36 %	25 %	15 %	8.2 %	4.3 %	2.6 %	2.0 %	2.1 %
	Neutral	0 %	0.02 %	0.02 %	0.03 %	0.05 %	0.05 %	0.06 %	0.07 %	/
	Settling	0 %	0 %	0 %	1.10^{-3} %	5.10^{-3} %	3.10^{-3} %	0 %	2.10^{-3} %	/
Autumn and Winter	Buoyant	36 %	21 %	17 %	8.6 %	4.7 %	2.2 %	1.3 %	0.92 %	0.64 %
	Neutral	0.19 %	0.21 %	0.21 %	0.25 %	0.65 %	0.27 %	0.28 %	0.25 %	0.28 %
	Settling	0 %	8.10^{-3} %	0.01 %	0.02 %	0.03 %	0.07 %	0.1 %	0.14 %	0.17 %

the MPs abundance in the water column. The regression model presented in the article offers a way to roughly correct this bias knowing the wind force and the water density. This regression model can also be improved by considering the season.

Thus, this simple model, based on a simplified hypothesis, provides very useful information on the analysis and interpretation of MPs distribution patterns in relation to hydrodynamic and climatic conditions. However, it could be improved in the future with more dedicated sampling in different layers and at the bottom.

Supplementary data to this article can be found online

CRediT authorship contribution statement

C. Chevalier: Conceptualization, Methodology, Software, Original draft preparation, Writing- Reviewing and Editing, Supervision, Numerical Resources, Formal analysis, Investigation

M. Vandenberghe: Validation, Original draft preparation, Investigation

M. Pagano: Writing- Reviewing and Editing

I. Pellet: Validation

C. Pinazo: Numerical Resources, Data curation, Writing- Reviewing and Editing

J. A. Tesán Onrubia, L. Guilloux: In-situ Resources

F. Carlotti: Funding acquisition, Project administration, Conceptualization, Supervision, Writing- Reviewing and Editing

Declaration of competing interest

The authors declare that they have no known competing financial interests or personal relationships that could have appeared to influence the work reported in this paper.

Data availability

Data will be made available on request.

Acknowledgments

This work was supported by the French National program EC2CO (Ecosphère Continentale et Côtière) by funding from the project Pelagoplastics (#°13082 Call EC2CO2020; PI: F. Carlotti).

Our thanks to the crew and Captain of the Antedon.

We are indebted to Michael Paul, a native English speaker, for proofreading the text. We would also like to acknowledge two anonymous reviewers for their constructive comments and suggestions.

References

Ahrens, J.P., 2000. A fall-velocity equation. J. Waterw. Port Coast. Ocean Eng. 126, 99–102.

Andrady, A.L., 2017. The plastic in microplastics: a review. Mar. Pollut. Bull. 119, 12–22.

Barnes, D., Galgani, F., Thompson, R., Barlaz, M., 2009. Accumulation and fragmentation of plastic debris in global environments. Philos. Trans. R. Soc. 364, 1985–1998.

Biber, N.F., Foggo, A., Thompson, R.C., 2019. Characterising the deterioration of different plastics in air and seawater. Mar. Pollut. Bull. 141, 595–602.

Brandon, J., Goldstein, M., Ohman, M.D., 2016. Long-term aging and degradation of microplastic particles: comparing in situ oceanic and experimental weathering patterns. Mar. Pollut. Bull. 110, 299–308.

Choi, C.E., Zhang, J., Liang, Z., 2022. Towards realistic predictions of microplastic fiber transport in aquatic environments: secondary motions. Water Res. 218, 118476.

Coyle, R., Hardiman, G., O'Driscoll, K., 2020. Microplastics in the marine environment: a review of their sources, distribution processes, uptake and exchange in ecosystems. Case Stud. Chem. Environ. Eng. 2, 100010.

Crawford, C.B., Quinn, B., 2016. Microplastic Pollutants. Elsevier Limited.

Daily, J., Hoffman, M.J., 2020. Modeling the three-dimensional transport and distribution of multiple microplastic polymer types in Lake Erie. Mar. Pollut. Bull. 154, 111024.

Defontaine, S., Sous, D., Tesan, J., Monperrus, M., Lenoble, V., Lanceleur, L., 2020. Microplastics in a salt-wedge estuary: vertical structure and tidal dynamics. Mar. Pollut. Bull. 160, 111688.

Enders, K., Lenz, R., Stedmon, C.A., Nielsen, T.G., 2015. Abundance, size and polymer composition of marine microplastics≥ 10 μm in the Atlantic Ocean and their modelled vertical distribution. Mar. Pollut. Bull. 100, 70–81.

Eriksen, M., Lebreton, L.C., Carson, H.S., Thiel, M., Moore, C.J., Borrero, J.C., Galgani, F., Ryan, P.G., Reisser, J., 2014. Plastic pollution in the world's oceans: more than 5 trillion plastic pieces weighing over 250,000 tons afloat at sea. PloS one 9, e111913.

Erni-Cassola, G., Zadjelovic, V., Gibson, M.I., Christie-Oleza, J.A., 2019. Distribution of plastic polymer types in the marine environment; a meta-analysis. J. Hazard. Mater. 369, 691–698.

Estournel, C., Durrieu de Madron, X., Marsaleix, P., Auclair, F., Julliand, C., Vehil, R., 2003. Observation and modeling of the winter coastal oceanic circulation in the Gulf of lion under wind conditions influenced by the continental orography (FETCH experiment). J. Geophys. Res. Oceans 108.

Fraysse, M., Pinazo, C., Faure, V., Fuchs, R., Lazzari, P., Raimbault, P., Pairaud, I., 2013. 3D coupled physicalbiogeochemical model development around Marseille's coastal area (NW Mediterranean Sea): what complexity is required in coastal zone. PloS one 8, e80012.

Fraysse, M., Pairaud, I., Ross, O.N., Faure, V.M., Pinazo, C., 2014. Intrusion of Rhone River diluted water into the bay of Marseille: generation processes and impacts on ecosystem functioning. J. Geophys. Res. Oceans 119, 6535–6556.

Gaspar, P., Grégoris, Y., Lefevre, J.M., 1990. A simple eddy kinetic energy model for simulations of the oceanic vertical mixing: tests at station papa and long-term Upper Ocean study site. J. Geophys. Res. Oceans 95, 16179–16193.

Hallermeier, R.J., 1980. A profile zonation for seasonal sand beaches from wave climate. Coast. Eng. 4, 253–277.

Hidalgo-Ruz, V., Gutow, L., Thompson, R.C., Thiel, M., 2012. Microplastics in the marine environment: a review of the methods used for identification and quantification. Environ. Sci. Technol. 46, 3060–3075.

Jambeck, J.R., Geyer, R., Wilcox, C., Siegler, T.R., Perryman, M., Andrady, A., Narayan, R., Law, K.L., 2015. Plastic waste inputs from land into the ocean. Science 347, 768–771.

Kedzierski, M., Palazot, M., Soccalingame, L., Falcou-Préfol, M., Gorsky, G., Galgani, F., Bruzaud, S., Pedrotti, M.L., 2022. Chemical composition of microplastics floating on the surface of the Mediterranean Sea. Mar. Pollut. Bull. 174, 113284.

Kedzierski, M., Palazot, M., Soccalingame, L., Falcou-Préfol, M., Gorsky, G., Galgani, F., Bruzaud, S., Pedrotti, M.L., 2022. Chemical composition of microplastics floating on the surface of the Mediterranean Sea. Mar. Pollut. Bull. 174, 113284.

Khatmullina, L., Chubarenko, I., 2021. Thin synthetic fibers sinking in still and convectively mixing water: laboratory experiments and projection to oceanic environment. Environ. Pollut. 288, 117714.

Khatmullina, L., Isachenko, I., 2017. Settling velocity of microplastic particles of regular shapes. Mar. Pollut. Bull. 114, 871–880.

Kooi, M., Koelmans, A.A., 2019. Simplifying microplastic via continuous probability distributions for size, shape, and density. Environ. Sci. Technol. Lett. 6, 551–557.

Kooi, M., Reisser, J., Slat, B., Ferrari, F.F., Schmid, M.S., Cunsolo, S., Brambini, R., Noble, K., Sirks, L.-A., Linders, T.E., 2016. The effect of particle properties on the depth profile of buoyant plastics in the ocean. Sci. Rep. 6, 1–10.

Kooi, M., Nes, E.H.V., Scheffer, M., Koelmans, A.A., 2017. Ups and downs in the ocean: effects of biofouling on vertical transport of microplastics. Environ. Sci. Technol. 51, 7963–7971.

Kukulka, T., Proskurowski, G., Morét-Ferguson, S., Meyer, D.W., Law, K.L., 2012. The effect of wind mixing on the vertical distribution of buoyant plastic debris. Geophys. Res. Lett. 39.

Lazure, P., Dumas, F., 2008. An external–internal mode coupling for a 3D hydrodynamical model for applications at regional scale (MARS). Adv. Water Resour. 31, 233–250.

Lebreton, L.-M., Greer, S., Borrero, J.C., 2012. Numerical modelling of floating debris in the world's oceans. Mar. Pollut. Bull. 64, 653–661.

Lefebvre, C., Saraux, C., Heitz, O., Nowaczyk, A., Bonnet, D., 2019. Microplastics FTIR characterisation and distribution in the water column and digestive tracts of small pelagic fish in the Gulf of lions. Mar. Pollut. Bull. 142, 510–519.

Lehtiniemi, M., Hartikainen, S., Näkki, P., Engström-Öst, J., Koistinen, A., Setälä, O., 2018. Size matters more than shape: ingestion of primary and secondary microplastics by small predators. Food Webs 17, e00097.

Lenaker, P.L., Baldwin, A.K., Corsi, S.R., Mason, S.A., Reneau, P.C., Scott, J.W., 2019. Vertical distribution of microplastics in the water column and surficial sediment from the Milwaukee River basin to Lake Michigan. Environ. Sci. Technol. 53, 12227–12237.

Li, Y., Wolanski, E., Dai, Z., Lambrechts, J., Tang, C., Zhang, H., 2018. Trapping of plastics in semi-enclosed seas: insights from the Bohai Sea, China. Mar. Pollut. Bull. 137, 509–517.

Maximenko, N., Hafner, J., Niiler, P., 2012. Pathways of marine debris derived from trajectories of Lagrangian drifters. Mar. Pollut. Bull. 65, 51–62.

Millet, B., Pinazo, C., Banaru, D., Pagès, R., Guiart, P., Pairaud, I., 2018. Unexpected spatial impact of treatment plant discharges induced by episodic hydrodynamic events: modelling lagrangian transport of fine particles by northern current intrusions in the bays of Marseille (France). PloS one 13, e0195257.

Millot, C., 1990. The gulf of Lions' hydrodynamics. Cont. Shelf Res. 10, 885–894.

Millot, C., 1992. Are there major differences between the largest Mediterranean Seas? A preliminary investigation. Bull. Inst. Océanogr. Monaco 3–25.

Nguyen, T.H., Tang, F.H., Maggi, F., 2020. Sinking of microbial-associated microplastics in natural waters. PloS one 15, e0228209.

Nguyen, T.H., Kieu-Le, T.-C., Tang, F.H., Maggi, F., 2022. Controlling factors of microplastic fibre settling through a water column. Sci. Total Environ. 838, 156011.

Nicolle, A., Garreau, P., Liorzou, B., 2009. Modelling for anchovy recruitment studies in the Gulf of lions (Western Mediterranean Sea). Ocean Dyn. 59, 953–968.

Onink, V., Wichmann, D., Delandmeter, P., van Sebille, E., 2019. The role of Ekman currents, geostrophy, and stokes drift in the accumulation of floating microplastic. J. Geophys. Res. Oceans 124, 1474–1490.

Pairaud, I., Gatti, J., Bensoussan, N., Verney, R., Garreau, P., 2011. Hydrology and circulation in a coastal area off Marseille: validation of a nested 3D model with observations. J. Mar. Syst. 88, 20–33.

Petrenko, A., Leredde, Y., Marsaleix, P., 2005. Circulation in a stratified and wind-forced gulf of lions, NW Mediterranean Sea: in situ and modeling data. Cont. Shelf Res. 25, 7–27.

Ross, O.N., Fraysse, M., Pinazo, C., Pairaud, I., 2016. Impact of an intrusion by the northern current on the biogeochemistry in the eastern gulf of lion, NW Mediterranean. Estuar. Coast. Shelf Sci. 170, 1–9.

Schmidt, N., Thibault, D., Galgani, F., Paluselli, A., Sempéré, R., 2018. Occurrence of microplastics in surface waters of the Gulf of lion (NW Mediterranean Sea). Prog. Oceanogr. 163, 214–220.

Schmidt, N., Fauvelle, V., Castro-Jiménez, J., Lajaunie-Salla, K., Pinazo, C., Yohia, C., Sempere, R., 2019. Occurrence of perfluoroalkyl substances in the bay of Marseille (NW Mediterranean Sea) and the Rhône River. Mar. Pollut. Bull. 149, 110491.

Van Sebille, E., Wilcox, C., Lebreton, L., Maximenko, N., Hardesty, B.D., Van Franeker, J. A., Eriksen, M., Siegel, D., Galgani, F., Law, K.L., 2015. A global inventory of small floating plastic debris. Environ. Res. Lett. 10, 124006.

Van Sebille, E., Delandmeter, P., Schofield, J., Hardesty, B.D., Jones, J., Donnelly, A., 2019. Basin-scale sources and pathways of microplastic that ends up in the Galápagos archipelago. Ocean Sci. 15, 1341–1349.

Tsiaras, K., Costa, E., Morgana, S., Gambardella, C., Piazza, V., Faimali, M., Minetti, R., Zeri, C., Thyssen, M., Ismail, S.B., 2022. Microplastics in the Mediterranean: Variability From Observations and Model Analysis. Cleaning Litter by Developing and Applying Innovative Methods in Eeropean Seas 16648714.

Van Sebille, E., Aliani, S., Law, K.L., Maximenko, N., Alsina, J.M., Bagaev, A., Bergmann, M., Chapron, B., Chubarenko, I., Cózar, A., 2020. The physical oceanography of the transport of floating marine debris. Environ. Res. Lett. 15, 023003.

Yohia, C., 2016. Genèse du mistral par interaction barocline et advection du tourbillon potentiel-«Vers Une nouvelle approche dynamique pour Une meilleure définition du maître des vents». Climatologie 13, 24–37.